ELSEVIER

Materials Science and Engineering A340 (2003) 68–79

MATERIALS SCIENCE & ENGINEERING A

www.elsevier.com/locate/msea

Effects of microstructural change on fracture characteristics in coarse-grained heat-affected zones of QLT-processed 9% Ni steel

Jae-il Jang [a,*], Jang-Bog Ju [b], Baik-Woo Lee [b], Dongil Kwon [b], Woo-Sik Kim [c]

[a] *Frontics, Inc., Research Institute of Advanced Materials, Seoul National University, Seoul 151-742, South Korea*
[b] *School of Materials Science and Engineering, Seoul National University, Seoul 151-742, South Korea*
[c] *Research and Development Center, Korea Gas Corporation, Ansan 425-150, South Korea*

Received 5 February 2001; received in revised form 22 February 2002

Abstract

This study investigates the correlation between the microstructural change and fracture characteristics in the coarse-grained heat-affected zones (CGHAZs) of the newly developed quenching, lamellarizing and tempering (QLT)-processed 9% Ni steel. The microscopic fracture behaviors of the various sub-zones within the HAZs including local brittle zone (LBZ) were estimated using simulated HAZ specimens. Both results of Charpy impact tests and in situ scanning electron microscopy (SEM) observations on simulated CGHAZ specimens show that the inter-critically reheated coarse-grained HAZ (IC CGHAZ) is a primary LBZ of this steel at cryogenic temperature, but not at room temperature. Microstructural analysis suggests that, unlike in other studies, the cryogenic LBZ phenomenon of the IC CGHAZs cannot be explained simply by the amount of martensite–austenite (M–A) constituents, but is mainly associated with the carbon contents in them. From all results obtained, a mechanism for microscopic toughness change among the CGHAZs is proposed and discussed.

Keywords: Coarse-grained heat-affected zone (CGHAZ); QLT-9% Ni steel; Microstructure; Fracture; Weld simulation; Local brittle zone (LBZ)

1. Introduction

Nine percent Ni steel has been widely used around the world as a material for the inner walls of liquefied natural gas (LNG) storage tanks because of its excellent cryogenic fracture toughness at or below 111 K, the boiling temperature of LNG. Nine percent Ni steels were generally processed by quenching and tempering (QT), double normalizing and tempering (NNT) or direct quenching and tempering (DQT) heat treatment. A new quenching, larmellarizing and tempering (QLT)-treated 9% Ni steel was developed [1] and has been used as an inner wall material in Korea because it exhibits better toughness and increased safety margin than the conventionally heat treated 9% Ni steel. The QLT process, originally developed for lower Ni steel such as 5.5% Ni steel [2], enhances cryogenic toughness considerably over other conventional processes. This effect is attributed to the refinement of effective grain size and the increased amount of stable austenite at cryogenic temperature.

During the construction of LNG storage tanks in Korea, the QLT-9% Ni steels are welded by shielded metal arc welding (SMAW) and submerged arc welding (SAW) processes at vertical and horizontal joints, respectively. The excellent fracture properties of the base material must be carefully reconsidered because, as well accepted, welding can seriously alter the metallurgical and mechanical properties of materials and generally causes degradations of the properties. Therefore, the proper evaluation of the fracture characteristics in the heat-affected zones (HAZs) of multi-pass welded QLT-9% Ni steel joints is very important in assessing the safety performance of LNG storage tanks. The present work was undertaken to clarify the relationship between microstructural change and fracture characteristics in QLT-9% Ni steel HAZs.

It is now widely recognized that a small zone of abnormally low fracture toughness, referred to as a local

* Corresponding author
E-mail address: jijang@frontics.com (J.-i. Jang).

0921-5093/02/$ - see front matter
PII: S0921-5093(02)00190-9

brittle zone (LBZ), can exist in the HAZs of multi-pass welded structural steels. In general, the coarse-grained HAZ (CGHAZ) adjacent to the fusion line has the lowest toughness among the various regions within a HAZ because of unfavorable microstructure such as large prior austenite grain size [3–7]. Metallographic analyses reveal that a CGHAZ can be roughly categorized into four characteristic zones according to the peak temperature of subsequent thermal cycles in a multi-pass welding procedure: (i) unaltered CGHAZ (UA CGHAZ), the region reheated above specific temperature of grain growth or not reheated at all, (ii) super-critically reheated CGHAZ (SCR CGHAZ), the region reheated above A_{C3}, (iii) inter-critically reheated CGHAZ (IC CGHAZ), the region reheated between A_{C1} and A_{C3}, and (iv) sub-critically reheated CGHAZ (SC CGHAZ), the region reheated below A_{C1}. Among them, the SCR CGHAZ is often treated as fine-grained HAZ (FGHAZ) due to its recrystallized fine grain size [8]. Many studies have been conducted on microscopic fracture characteristics in these CGHAZs for the various structural steels, used mainly for offshore structures [3–7]. However, for a cryogenic steel such as 9% Ni steel, there have been few studies on the microstructures and fracture behaviors of the CGHAZs, and far fewer researches are available for QLT-9% Ni steel HAZ.

This paper describes the fracture properties of sub-regions of the CGHAZs using the results of Charpy impact tests and in situ scanning electron microscopy (SEM) observations. Then, the effects of microstructural change on the fracture behaviors are proposed by the metallurgical analysis.

2. Experimental

2.1. Material

The composition and basic mechanical properties of the material used in this study are given in Table 1. The 9% Ni steel was a commercial grade used for LNG storage tanks in Korea. The plates were normally processed by the QLT (Q: 1093 K for 60 min, quench, L: 963 K for 80 min, quench, and T: 853 K for 60 min, quench) heat treatment. The microstructures of the base metal consisted mainly of tempered martensite with 7–10 vol.% of retained austenite.

2.2. Welding simulation and fracture test

Weld simulations were performed for a systematic and reproducible investigation of the relationship between microstructural change and toughness variation within HAZ. Oversized Charpy specimen blanks (11 × 11 × 60 mm) were thermally cycled in a metal thermal cycle simulator (MTCS). The oversized dimension allowed removal of the surface oxide formed during the thermal cycling. A schematic illustration of the simulation profile is shown in Fig. 1. The thermal cycle for weld simulation is generally characterized both by the peak temperature (T_P) and the cooling time from 1073 to 773 K ($\Delta t_{8/5}$) or from 773 to 573 K ($\Delta t_{5/3}$), and $\Delta t_{5/3}$ is generally three times as long as $\Delta t_{8/5}$. After reaching the first peak temperature at 1623 K, the specimens were cooled down with the constant cooling time ($\Delta t_{8/5}$) of 13.5 and 19.4 s and the cooling rates were approximately equivalent to those of a SAW and a SMAW with heat inputs of 23 and 28 kJ cm^{-1}, respectively, in a 22 mm thick plate. These simulated welding conditions were based on the actual welding conditions used in welding of the tanks in Korea, and calculated through a modified equation based on Rosenthal's heat-flow equation [9]. The peak temperature of the second weld thermal cycle, T_{P2}, was varied between 1473 and 823 K for the thermal cycle simulating the second weld bead. The cooling rates of the second thermal cycle were the same as that of the first thermal cycle. To classify the CGHAZs according to the second peak temperature, dilatometry tests were also conducted.

The simulated specimen blanks were machined and notched to the final dimensions of the standard 2 mm V-notched Charpy specimen. The notch was located very close to the region where the thermocouple was attached during the simulation test. Charpy impact tests were

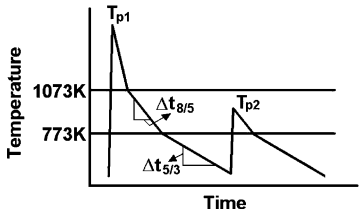

Fig. 1. Typical simulation profile for double thermal cycles when the cooling rate is maintained constant during the cycles.

Table 1
Chemical compositions and mechanical properties of QLT-9% Ni steel

Chemical compositions (wt.%)						Mechanical Properties at R.T. (at 77 K)			
C	Si	Mn	P	S	Ni	YP (MPa)	TS (MPa)	EL (%)	Charpy E (J)
0.066	0.24	0.65	0.005	0.005	9.28	640 (910)	720 (1140)	36 (34)	293 (227)

performed at room temperature (R.T.) and 77 K, the temperature of liquid nitrogen. More than three specimens were tested for each condition, and average values were used for this work. Since the simulated specimens for each condition had a single microstructure, there was little scatter of impact values for a given condition. Also, the fracture surfaces of the specimens were observed by SEM.

To observe the fracture behaviors of the simulated CGHAZ specimens, in situ fracture observations of the simulated specimens were conducted using a tensile loading stage within the SEM. For the in situ test, miniaturized single edge notched tension (SENT) specimens were prepared as shown in Fig. 2. The central groove part of the specimen was made thin so that it could be easily fractured under a light load. A sharp notch with a radius of about 30 μm similar to that of a fatigue pre-crack was made by electric discharge machine using a thin electric wire cutter, as shown in Fig. 3. The loading rate for the in situ testing was 0.032 mm s^{-1}. Since the specimens were not tested in the plane strain condition because of the existence of central groove as shown in Fig. 2, valid K_{IC} values were not obtained. The apparent fracture toughness under plane stress condition, K_C, were obtained using the stress intensity factor for SENT specimen. The related equations were as follows:

$$K_C = \frac{P_{max}}{B\sqrt{W}} f\left(\frac{a}{W}\right) \quad (1)$$

and

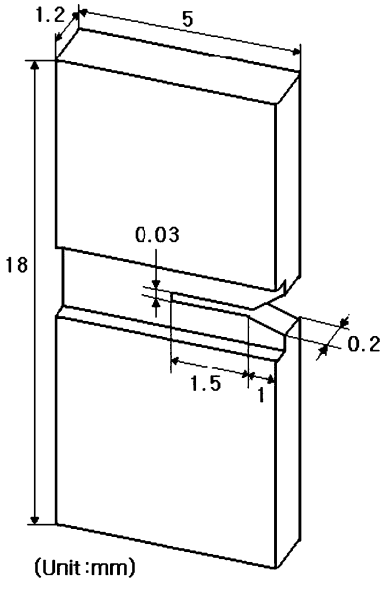

Fig. 2. Schematic diagram of miniaturized SENT specimens used in in situ observation.

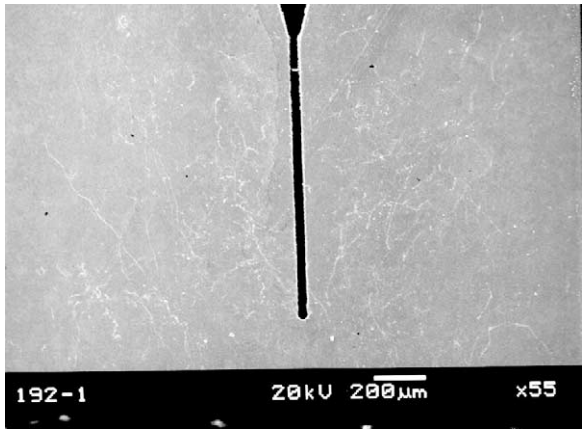

Fig. 3. An example of precrack width of about 30 μm made in SENT specimens.

$$f\left(\frac{a}{W}\right) = \frac{\sqrt{2\tan \pi a/2W}}{\cos \pi a/2W} \times \left[0.752 + 2.02\left(\frac{a}{W}\right) + 0.37\left(1 - \sin\frac{\pi a}{2W}\right)^3\right] \quad (2)$$

where P_{max}, B, W and a are the maximum load, specimen thickness, specimen width and crack length, respectively.

2.3. Metallographic examination

All samples in this investigation were prepared for metallographic examination using standard techniques such as optical microscopy, SEM, X-ray diffractometry (XRD), and electron probe X-ray micro-analysis (EPMA). Two percent Nital was used as chemical etchant for viewing under the optical microscope. XRD with CrK_α was used to determine the amount of retained austenite by comparing the integrated peak intensities of the $(200)_\alpha$ and $(220)_\gamma$ planes. For the observation of martensite–austenite (M–A) constituents, the two-stage electrolytic etching, a method developed by Ikawa et al. [10] was applied prior to SEM observation. The area fraction of the M–A constituents was measured by image analyzer, and the carbon contents in the M–A constituent were analyzed by EPMA.

3. Results and discussion

3.1. Fracture properties of simulated HAZ

The results of the Charpy impact tests at R.T. are shown in Fig. 4, as a function of the peak temperature of

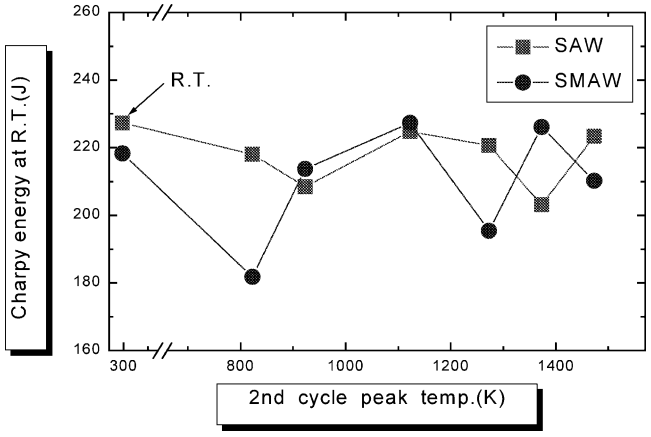

Fig. 4. Relation between Charpy impact energy at R.T. and the second peak temperature.

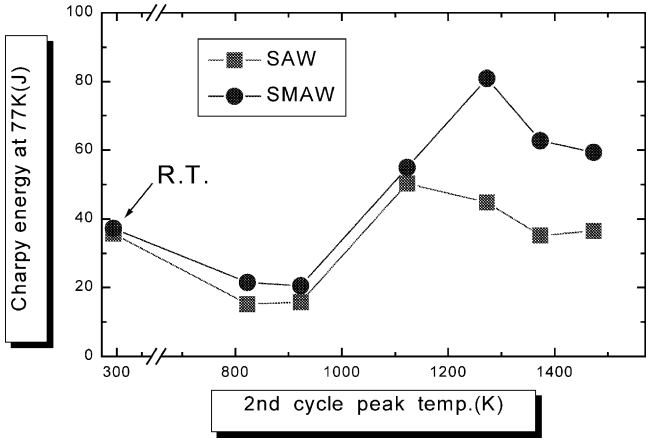

Fig. 5. Relation between Charpy impact energy at 77 K and the second peak temperature.

the second thermal cycle. Dilatometry test results showed that A_{C1} and A_{C3} were about 838 and 968 K. They might have been lowered because of the rapid thermal cycle during welding. Thus, the second thermal cycles with peak temperatures between 1473 and 1373 K were considered to simulate the UA CGHAZ while the cycles between 1273 and 1073 K simulate the SCR CGHAZ, and the cycles between 923 and 823 K simulate the IC CGHAZ, respectively. The SC CGHAZ was not considered in this study because the properties of the SC CGHAZ were expected to be similar or superior to those of the UA CGHAZ due to its low peak temperature and tempering effects. Although the impact values of the specimens at R.T. were lower than 293 J of the base metal as listed in Table 1, all specimens exhibited a moderate impact toughness near 200 J. Also, no clear tendency of change in toughness with the peak temperature of the second thermal cycle was formed. Therefore, it was concluded that there was no LBZ in the CGHAZs at R.T.

Since 9% Ni steel is generally used at cryogenic temperature, the cryogenic toughness of this steel is more important than the toughness at R.T. The Charpy impact test results at 77 K using the simulated CGHAZ specimens are shown in Fig. 5. Unlike the Charpy values at R.T., the results at 77 K show a large decrease in impact values from that of base metal, i.e. about 217 J at 77 K as listed in Table 1, and a clear tendency of change in impact values in both cases of SMAW and SAW. The CGHAZs exhibit low Charpy impact energies in two cases: IC CGHAZ and UA CGHAZ. Otherwise, the specimens simulating the SCR CGHAZs show the highest values. Specifically, values of the simulated IC CGHAZs for both SMAW and SAW are lower than the minimum impact value of the 'improved' 9% Ni steel at 77 K, 35 J, as required in the various standards [11,12]. Since the trends of toughness variation are nearly identical in both SMAW and SAW samples, probably due to the similar cooling rates, the results of the SMAW case will be discussed in the following sections of this paper.

The fractographs of the tested specimens at 77 K are shown in Fig. 6. From the fractographs, it is easily seen that the fracture of the IC CGHAZ specimens occurs by intergranular mode and the UA CGHAZ specimens fracture by transgranular mode. On the other hand, the SCR CGHAZ specimens with the highest impact value fracture by the mixed mode of localized quasi-cleavage and mainly ductile dimple rupture. This change in fracture mode is consistent with the change in impact toughness.

Consequently, it is possible to correlate that the IC CGHAZ is the primary LBZ of QLT-9% Ni steel and the UA CGHAZ might be the secondary LBZ. It is very interesting to note that the LBZs in the QLT-9% Ni steel appear only at cryogenic temperature, while the LBZs of other structural steels occur in the IC CGHAZs in most cases, and are associated with the lowest impact energy over the entire testing temperature range [3–7]. Therefore, the authors propose to call the microscopic embrittlement phenomenon of the IC CGHAZs as 'cryogenic LBZ phenomenon' and analyze such phenomenon in the following sections.

3.2. Microstructural analyses

To find the metallurgical factors controlling the cryogenic LBZ phenomenon, microstructural analyses were performed on the simulated CGHAZ specimens. First, the microstructures of the simulated CGHAZs were observed by optical microscopy. As shown in Fig. 7, the UA and IC CGHAZs consist of still coarsened microstructure of prior austenite grains and martensite laths. On the other hand, the SCR CGHAZs have fine grains because, as mentioned before, the second thermal cycle above A_{C3} changed the coarse grained microstructure to the fine grained microstructure through recrystallization [8]. Although the change in grain size

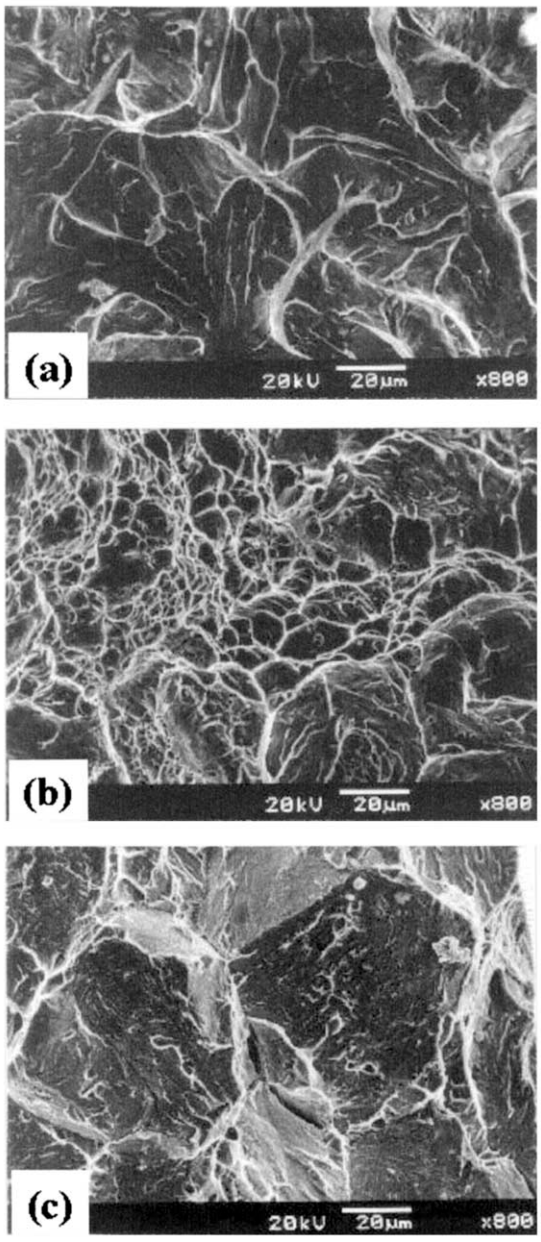

Fig. 6. SEM fractographs of Charpy tested specimens at 77 K; (a) simulated UA CGHAZ, (b) simulated SCR CGHAZ, and (c) simulated IC CGHAZ.

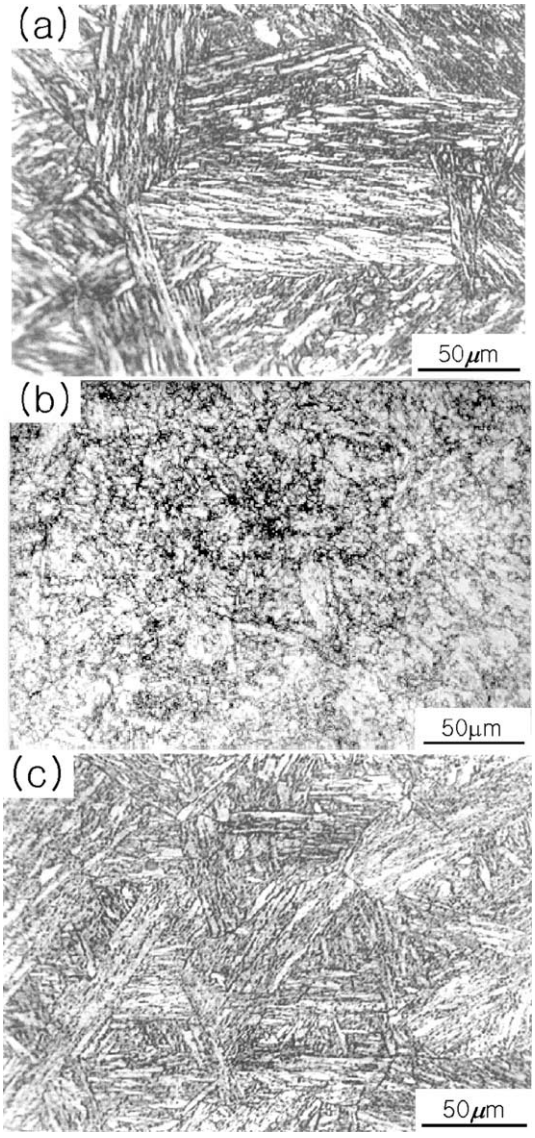

Fig. 7. Optical micrographs of the (a) simulated UA CGHAZ, (b) simulated SCR CGHAZ, and (c) simulated IC CGHAZ.

may be correlated to the highest toughness of the SCR CGHAZs among the CGHAZs, the grain size variation alone could not account for the difference in toughness between the UA CGHAZs and the IC CGHAZs.

The amount of retained austenite was measured in samples used for the impact test specimens with them Charpy values shown in Figs. 4 and 5. As with the grain refinement, retained austenite is widely known as one of the most important factors affecting the cryogenic toughness of 9% Ni steel [1,13,14]. The base material of QLT-9% Ni steel was found to contain 7–10 vol.% of retained austenite. Fig. 8 shows examples of the retained austenite measurement by XRD on the impact specimens tested at 77 K. At where a peak for austenite might rise if it existed, there was no austenite peak is observed at about $2\theta = 130^\circ$ in all of the specimens while an α-Fe peak appears at about $2\theta = 106^\circ$. All samples of the CGHAZs showed the same results. These results are well consistent with the results of a previous study [15] using the actual HAZ specimens of QLT-9% Ni steel. In the study [15], the average volume fraction of retained austenite in the areas near the fusion line, i.e. the areas of mostly CGHAZs, was less than 1%. Therefore, it is obvious that the change in the amount of retained austenite is not the governing factor of toughness change because the amount of retained austenite is very low in the CGHAZs. The absence of retained austenite is due to the rapid welding thermal cycle, as will be described below.

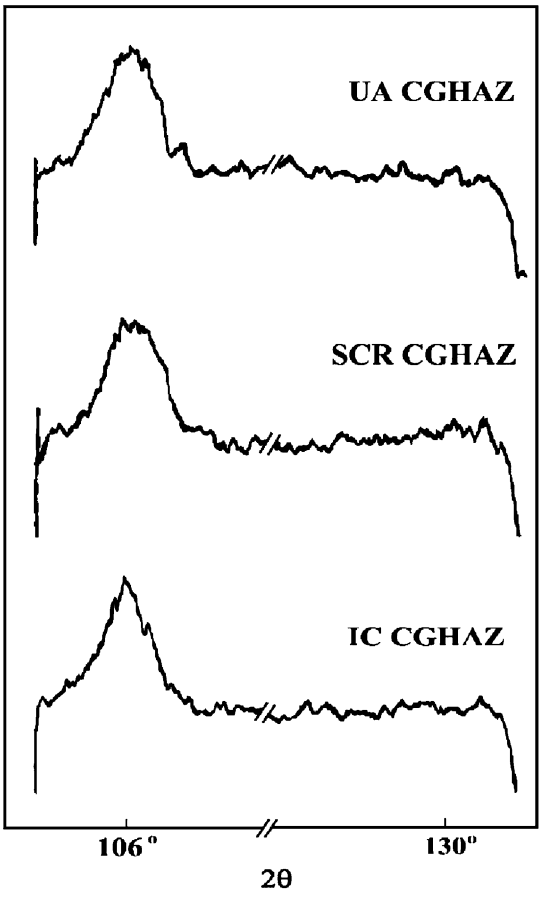

Fig. 8. Examples of XRD results for the simulated CGHAZ specimens.

Using the two-stage electrolytic etching method [10], the M–A constituents, sometimes called martensite islands, were observed in all specimens that simulated the CGHAZs. The M–A constituent, a microstructure with high carbon contents and thus high hardness value, is generally known as one of the main factors that reduce the toughness of the HAZs in high strength structural steel [3–7]. Fig. 9 shows some examples of the observed M–A constituents in the HAZs. The M–A constituents appear white in the SEM micrographs. The average width of the M–A constituents is 0.2–0.3 μm and the length is about several μm. Relatively small size of the M–A constituents in the simulated SCR CGHAZ is due to the fine-grained microstructures in the SCR CGHAZ. The existence of the M–A constituents rather than retained austenite in the CGHAZs was basically caused by the rapid welding thermal cycle. On reheating a CGHAZ above A_{C1}, austenite nucleated and grew preferentially along the prior austenite grain boundaries and martensitic lath boundaries. However, since there was insufficient time for the diffusion of substitutional elements, mainly Ni, the austenite became enriched only in the interstitial element, i.e. carbon. Therefore, on cooling, the austenite island had to transform to the M–A constituents along the prior austenite grain and lath boundaries [4–6].

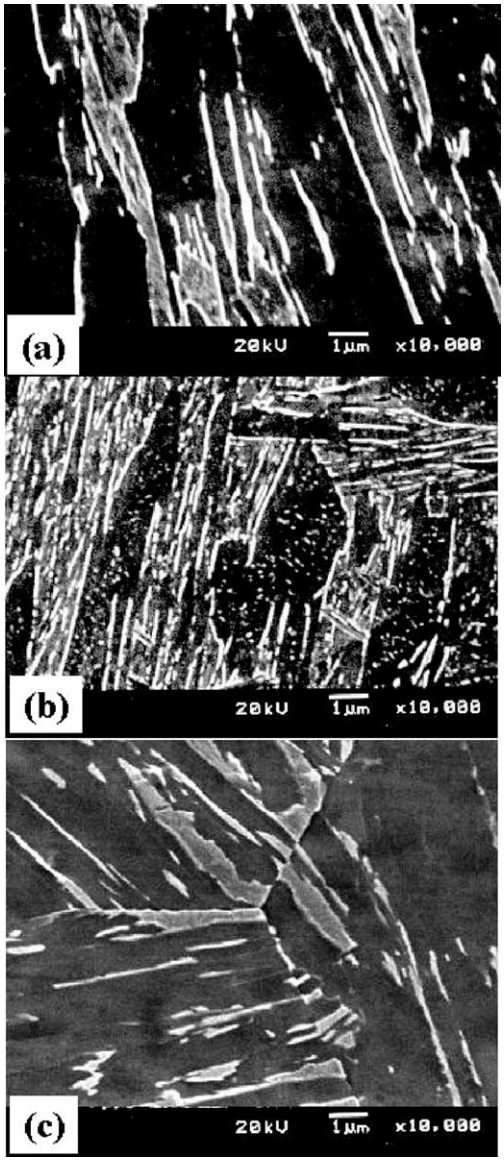

Fig. 9. Scanning electron micrographs in the simulated CGHAZ specimens prepared by 2-stage electrolytic etching technique [10] to observe M–A constituents; (a) simulated UA CGHAZ, (b) simulated SCR CGHAZ, and (c) simulated IC CGHAZ.

In all of the simulated CGHAZs, the area fraction of M–A constituents was measured by image analyzer using the specimens with and without sub-zero treatment at 77 K. Fig. 10 shows the M–A area fraction in the simulated UA, SCR and IC CGHAZs. The M–A fraction shows the minimum value in the SCR CGHAZs and similar values in the UA CGHAZs and the IC CGHAZs. In addition, the difference in the M–A fractions between the sub-zero treated and untreated specimens is very small. Comparing the change in the M–A fraction with the Charpy energy variation, it is evident that the cryogenic LBZ phenomenon of the IC

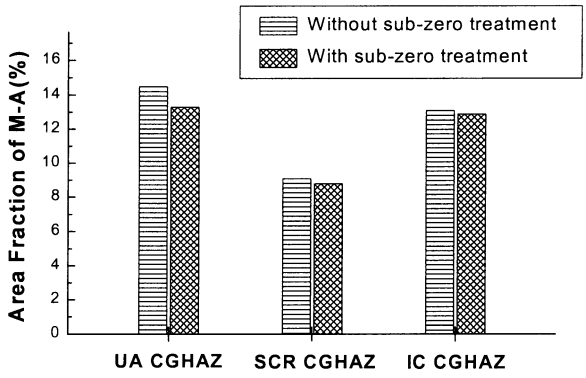

Fig. 10. Change in area fraction of M–A constituents in the simulated CGHAZs.

CGHAZs cannot be explained by the change in M–A area fraction alone.

The authors also attempted to estimate the change in the hardness of M–A constituents in all simulated CGHAZ specimens. However, even with a small load of 0.1 g, hardness of the M–A constituents was not measurable because the size of the M–A constituents was too small. To overcome this problem, EPMA was used to estimate the carbon contents in the M–A constituents, considering the fact that carbon content is generally known as an effective indicator on the hardness of the martensite phase. So, carbon contents in the M–A constituents of each CGHAZ specimen were evaluated quantitatively by EPMA. Fig. 11 shows the representative examples of EPMA results, and Table 2 lists the average value of the carbon contents. As shown in the figure and table, the results of EPMA exhibit the maximum and minimum carbon contents for the IC CGHAZ and the UA CGHAZ, respectively. From the results, it could be expected that the M–A constituents in the IC CGHAZ are of the highest hardness among the various CGHAZs. Conversely, the M–A constituents in the UA CGHAZs are of the lowest hardness.

The carbon content variation could be explained by the difference in the peak temperature during the second thermal cycle, as schematically illustrated in Fig. 12. As mentioned before, austenite islands enriched only in carbon are formed instead of normal austenite during the rapid reheating in the second thermal cycle. When the peak temperature of the second thermal cycle (T_{P2}) is between A_{C1} and A_{C3}, as in the case of IC CGHAZs, carbon concentration of the islands (C_1 in Fig. 12) is much higher than that of the matrix (C_0 in Fig. 12). When T_{P2} is above A_{C3}, as in the case of SCR CGHAZs, austenite islands would form at high carbon areas such as prior austenite grain boundaries from which carbon atoms would diffuse out but could not because the temperature is not high enough to provide the necessary mobility. Thus, carbon concentration in the austenite islands would be at a level between C_0 and C_1. When T_{P2} is above the grain growth temperature, as in the case of UA CGHAZs, austenite islands would grow, and at the same time, martensitic microstructures of matrix will also transform to austenite. So, the rediffusion of carbon from austenite islands to matrix would make the average carbon content in the islands of UA CGHAZs smaller than those of SCR CGHAZs.

During the cooling sequence, the carbon-enriched austenite islands have to transform mostly to martensite islands, i. e. M–A constituents, and the carbon concentration of the islands increases. It is due to the fact that the carbon in martensite matrix diffuses to neighboring islands, which results from insufficient time for long-range diffusion. Generally, supercooling by rapid cooling rate raises the maximum carbon contents up to the value in extrapolated austenite/(austenite+ferrite) line of Fe–C diagram at the cooling temperature. Nakao et al. [16], calculating the carbon concentration using the width of M–A constituents, reported that the increased value would be over 1.5 wt.%. In the present work, the carbon content of about 2.2 wt.% in the case of IC CGHAZ is very high compared with the carbon content of the base metal, about 0.06 wt.%. However, the carbon content of 2.2 wt.% is within the range of the previous works that showed the carbon contents in the M–A constituents could be up to 2.6 wt.% [17,18], or at least consistent with the assertion that there is no relationship between carbon contents in the base material and those in the M–A constituents [19].

3.3. *In situ observation of fracture behavior*

To examine the difference between the fracture behaviors at R.T. and at cryogenic temperatures, in situ SEM fracture observations were performed using simulated CGHAZ specimens. In the case of fracture procedures at 77 K, the specimens were in situ tested within 30 s after the sub-zero treatment at 77 K since the direct observation in liquid nitrogen was very difficult. Since the specimens were under plane stress condition, as described above, the fracture surfaces of these specimens showed increased tendency of ductile fracture compared with those of larger-sized specimens such as Charpy impact specimens. Thus an increased apparent toughness, K_C, could be obtained instead of a valid plane strain fracture toughness, K_{IC}. Unfortunately, the microscopic crack initiation behaviors near the M–A constituents, such as formation of micro-voids or micro-cracks, could not be observed in the in situ tests due to the very small scale of the M–A constituents and the loading fluctuation of the system.

Fig. 13 shows a series of SEM micrographs of an IC CGHAZ specimen at R.T. without sub-zero treatment. As shown in the figure, the fracture was accompanied with a severe deformation. Fig. 14 shows a magnified view of a local area near the notch tip. Heavy deformation occurred in the matrix between neighboring M–A

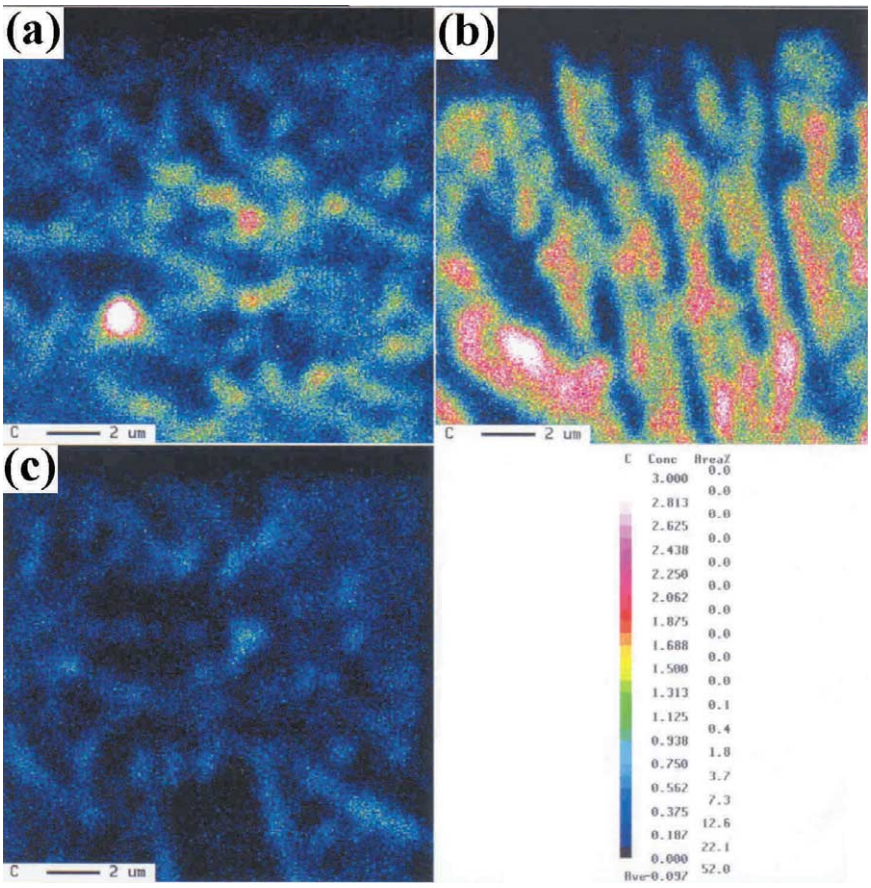

Fig. 11. Results of EPMA estimation of the carbon contents in the M–A constituents of simulated CGHAZ; (a) simulated SCR CGHAZ, (b) simulated IC CGHAZ, and (c) simulated UA CGHAZ.

Table 2
Change in carbon content in M–A constituents

Sub-region	C% in M–A
UA CGHAZ	0.75 wt.%
SCR CGHAZ	1.1 wt.%
IC CGHAZ	2.2 wt.%

constituents. The apparent fracture toughness, K_C, calculated from the maximum load is 162.19 MPa $(m)^{1/2}$. On the other hand, Fig. 15 shows a series of SEM micrographs for a sub-zero treated IC CGHAZ specimen. Although the specimen was under plane stress condition, a complete brittle fracture was observed. From the magnified micrographs in Fig. 16, it can be verified that there was no deformation, and some M–A constituents were fractured by brittle crack propagation. The apparent fracture toughness, K_C, calculated from maximum load is 108.78 MPa $(m)^{1/2}$. Other specimens simulating the UA CGHAZ and SCR CGHAZ exhibited ductile fracture behaviors similar to the simulated IC CGHAZ specimen which was not sub-zero treated. In the case of the UA CGHAZ, the absence of transgranular cleavage fracture observed in the Charpy test results is due to the increased tendency of ductile fracture under the plane stress condition.

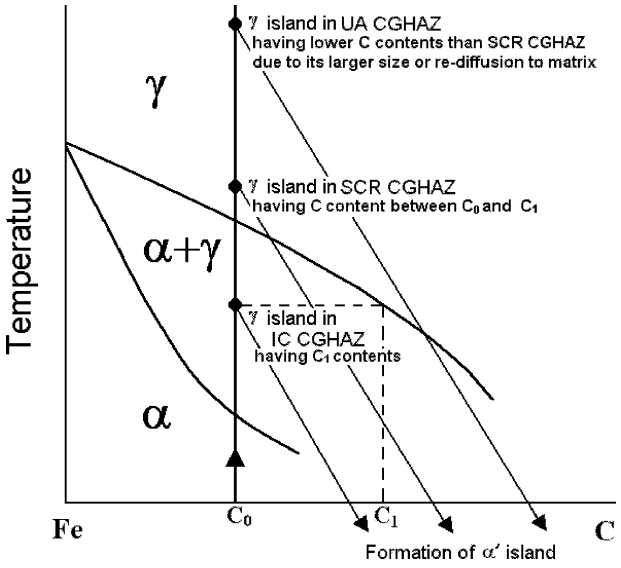

Fig. 12. Schematic diagram to explain a mechanism for the variation of carbon content in the M–A constituents in the CGHAZs during the reheating cycle sequence.

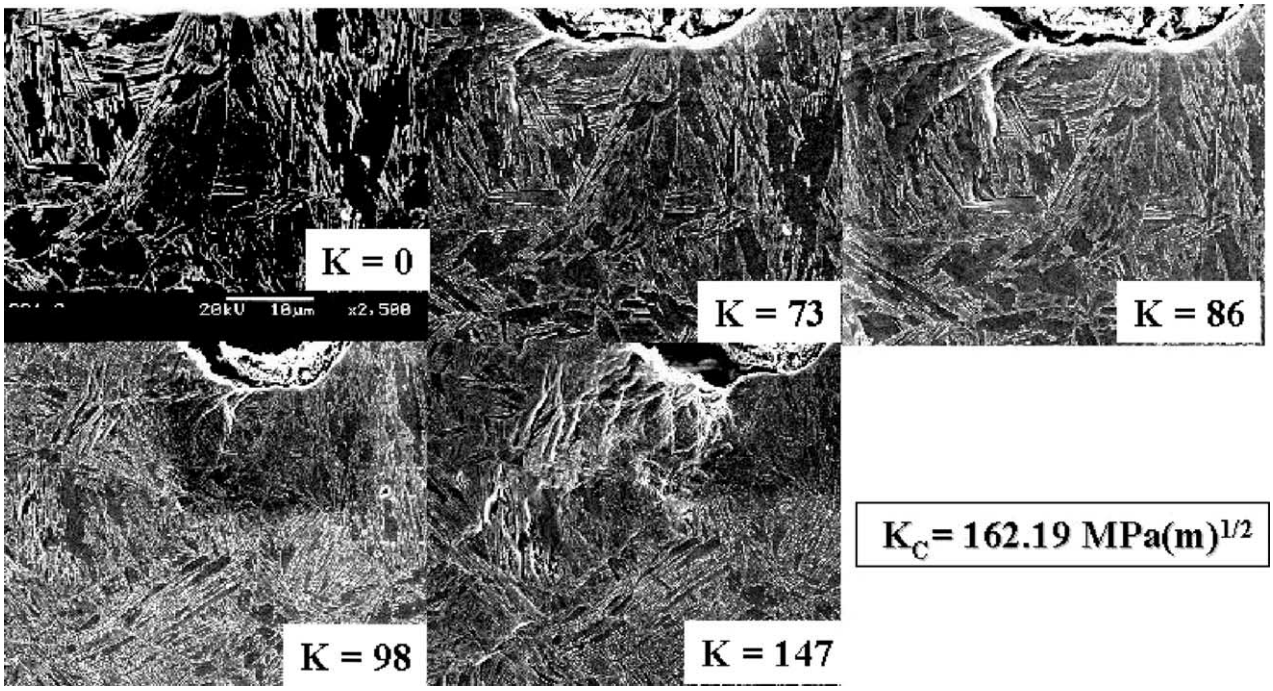

Fig. 13. A series of SEM micrographs near the notch tip region of a simulated IC CGHAZ specimen without sub-zero treatment.

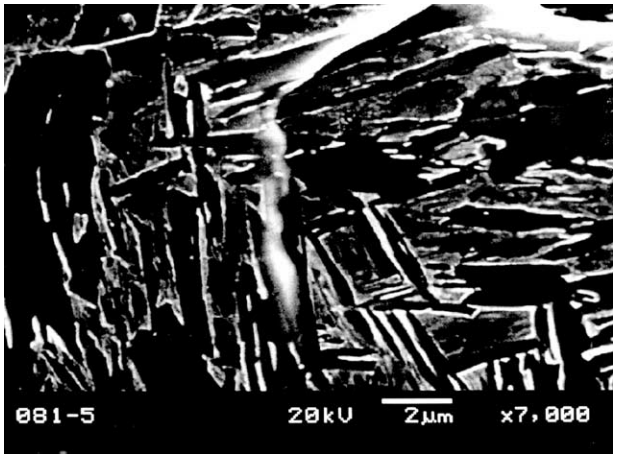

Fig. 14. Magnified SEM micrograph of a fracture sequence in Fig. 13.

Fig. 17 shows examples of the load-displacement curves from the in situ fracture tests. The curve for the sub-zero-treated IC CGHAZ indicates not only the lowest apparent fracture toughness but also the absence of stable crack growth. It is also noted that both the maximum load and displacement value at the maximum load point in the sub-zero treated IC CGHAZ specimen were much lower than those in other specimens. Therefore, the differences between the brittleness of the IC CGHAZs at R.T. and at cryogenic temperature can be mainly attributed to the change in fracture mode, even though the miniaturized SENT specimen was under plane stress condition.

3.4. Mechanism of cryogenic LBZ

The purpose of this section is to obtain an valuable insight into the mechanism of microscopic toughness variation among the CGHAZs of QLT-9% Ni steel. Although M–A constituents were observed in all of the simulated CGHAZ samples in this study, the cryogenic LBZ phenomenon of IC CGHAZ could not be explained by the change in the area fraction of M–A alone. This result is of a great interest, since the amount of the M–A constituents has been treated until now as the most important factor in the LBZ phenomenon of the IC CGHAZ in many studies on high strength structural steel HAZs [3–7]. Therefore, for the interpretation of the cryogenic LBZ mechanism, the role of M–A constituents at test temperatures is considered in detail from the view point of strength mismatch between the M–A constituents and neighboring matrix. Then, the microscopic toughness variation among the CGHAZs could be explained by the following mechanisms.

Although the M–A fraction in the IC CGHAZs is a little smaller than that in the UA CGHAZs, the M–A constituents in the IC CGHAZs contain a much higher carbon content of about 2.2% than that in the UA CGHAZs. Hrivnak et al. [20] suggested the empirical relationship for the M–A constituents between their Vickers hardness (H_{M-A}) and carbon content (C wt.%) as follows:

$$C\ (\text{wt.}\%) = \frac{(H_{M-A} - 15)}{575} \quad (3)$$

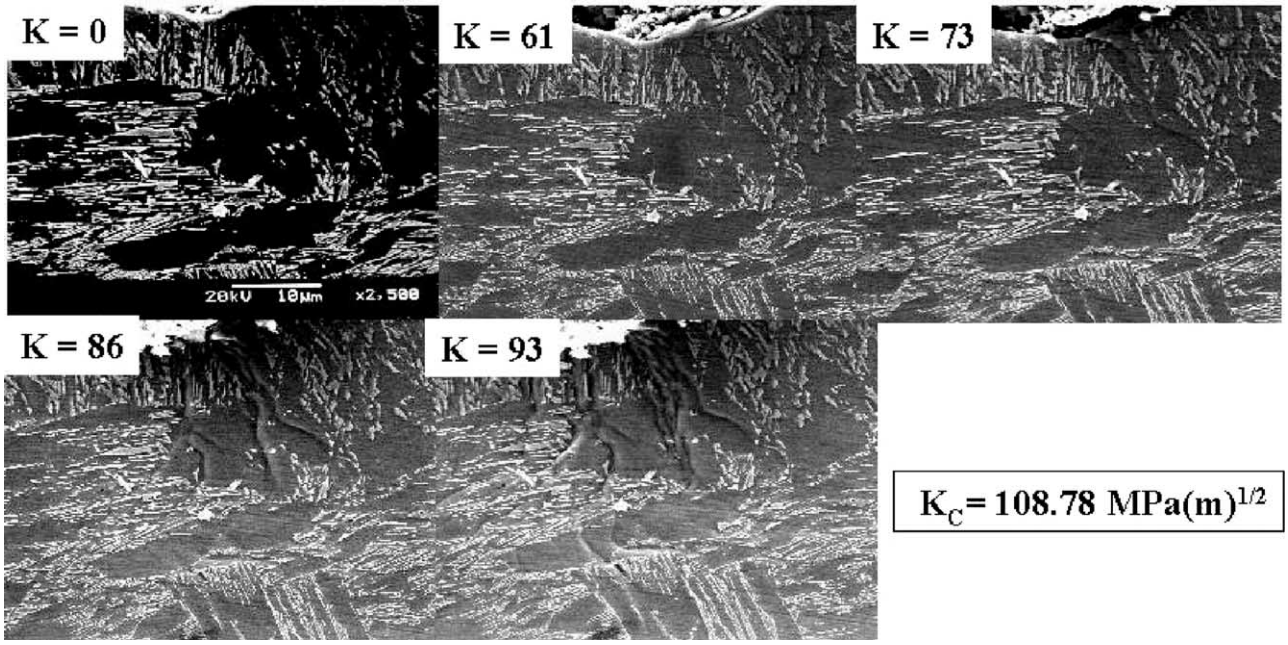

Fig. 15. A series of SEM micrographs near the notch tip region of a simulated IC CGHAZ specimen which was sub-zero treated at 77 K.

Fig. 16. Magnified SEM micrograph of a fracture sequence in Fig. 15.

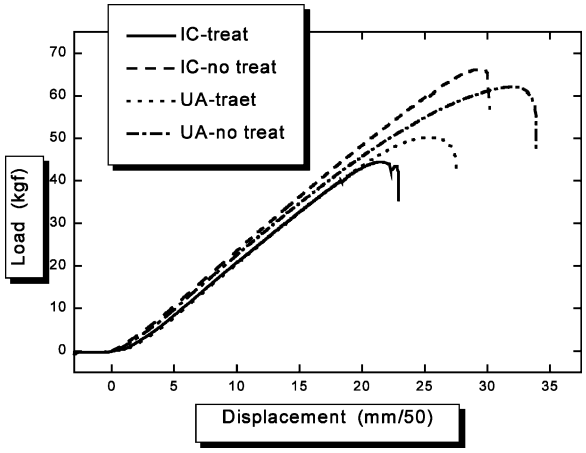

Fig. 17. Load vs. displacement curves from the in situ fracture tests using miniaturized SENT specimens (IC: simulated IC CGHAZ, UA: simulated UA CGHAZ, treat: sub-zero treated specimen, no treat: untreated specimen).

Although the exact value of hardness cannot be obtained from the above equation, the relative change in hardness among the CGHAZs can be evaluated. In the cases of UA CGHAZs and SCR CGHAZs, the calculated hardness values of the M–A constituents are 447 and 648H_V, respectively. However, in the case of IC CGHAZs, it is about 1280H_V. Since the average hardness of the HAZ in the QLT-9% Ni steel is about 400H_V as found in a previous work [1], it can be recognized that the IC CGHAZs have the largest strength mismatch between the M–A constituents and matrix among the CGHAZs while UA CGHAZ have almost no mismatch between them.

Chen et al. [21] propose that the stress concentration and triaxiality of the neighboring matrix are increased by the hard phase particles such as the M–A constituents and that the stress in the neighboring matrix can be elevated to several times the average stress. With this suggestion, the matrix surrounding the M–A constituents in the IC CGHAZ of this steel can be plastically constrained more than other CGHAZs. At R.T., it is relatively easy for the matrix to deform plastically, and the elevated stress can be relieved. Thus a heavy deformation may occur in the matrix between the neighboring M–A constituents, as shown in Figs. 13 and 14. In contrast, at cryogenic temperature, the plastic deformation of the matrix may not be easy and thus the high stress concentration and triaxiality cannot be relieved. In this situation, brittle cracking can occur from the M–A constituents along the relatively weak boundaries and propagate, as shown in Figs. 15 and 16.

The difference in fracture behavior at 77 K and at R.T. can be also explained by the difference in plastic zone size, since the plastic zone size is directly related to toughness [22]. From Irwin's approach [23], the plastic zone sizes of the IC CGHAZ specimens at RT and 77 K can be roughly calculated using both K_C values (obtained from the in-situ fracture tests) and yield strengths of IC CGHAZ (predicted from base-metal yield strengths and hardness comparison between IC CGHAZ and base metal). These calculations reveal that the plastic zone size of the miniaturized SENT specimen at R.T. (about 10–15 mm) is at least five times greater than that at 77 K (about 1–2 mm). It is thus understandable that a large amount of energy is dissipated during crack propagation at R.T., while crack propagation at 77 K requires significantly less energy.

On the other hand, in the case of UA CGHAZs, although the M–A fraction is a little larger than that in the IC CGHAZs, a significant increase in the stress does not exist in the matrix. This is because the carbon content in the M–A constituents is very low, 0.75%, in comparison with the M–A constituents in other CGHAZs, and thus there is little microscopic strength mismatch between the M–A constituents and the matrix. Therefore, the main factor affecting toughness decrease in the UA CGHAZs at cryogenic temperature is not the existence of M–A constituents, but the coarse grain size and absence of the retained austenite. Finally, in the case of SCR CGHAZs, the moderate toughness is mainly due to the fine-grained microstructure formed during the second thermal cycle with a peak temperature in the recrystallization range. In addition, the relatively small fraction of the M–A constituents assists the relatively high toughness. Consequently, although the M–A constituents in the SCR CGHAZ are harder than those in the UA CGHAZs due to the high carbon contents in M–A, the fine grain size and the small volume fraction of the M–A constituents result in the higher toughness of the SCR CGHAZs.

4. Conclusions

The microstructural effects on the fracture characteristics of QLT-9% Ni steel HAZ were investigated using simulated HAZ specimens. The primary results of this investigation are: (1) among the coarse-grained HAZs, the IC CGHAZ is found to have the lowest toughness value at 77 K, indicating that it is the primary LBZ at a cryogenic temperature, at which 9% Ni steel is generally used, but is not at R.T. (2) The impact toughness variation of the simulated CGHAZ specimens could not be explained by the change in volume fraction of the retained austenite, a factor known as the most important metallurgical factor controlling the cryogenic toughness of 9% Ni steel. Instead, the M–A constituents were observed to form along the boundaries of laths or prior austenite grains. Microstructural analyses of the M–A constituents revealed that the M–A constituents in the IC CGHAZ have much higher carbon contents than in other CGHAZs such as UA CGHAZ and SCR CGHAZ, although the amount of M–A constituents in the UA CGHAZ is a little larger than in the IC CGHAZ. Additionally, the clear difference in fracture behavior at cryogenic and room temperatures was verified by the in situ observation of the simulated IC CGHAZ. (3) Based on the results obtained, a mechanism of the cryogenic LBZ phenomena was discussed and proposed. In the case of IC CGHAZ, the M–A constituents containing high carbon content can raise the stress of neighboring matrix and thus can easily induce the brittle fracture at cryogenic temperature. Although the UA CGHAZ has a slightly larger amount of M–A constituents than the IC CGHAZ, it shows a higher toughness than the IC CGHAZ mainly because its M–A constituents have a too small carbon content to critically raise the stress of the neighboring matrix. On the other hand, the high toughness of the SCR CGHAZ was attributed to the fine-grained microstructure and small fraction of the M–A constituents.

It is hoped that this work using the simulated HAZ specimens will be valuable in interpreting microscopic fracture characteristics in QLT-9% Ni steel HAZs. However, it should be also noted that there could be difficulties in direct extrapolation of these results to actual weld joints, since there are additionally considerable factors. For example, the plastic zone size near the crack tip front could be larger than the LBZ even at 77 K. So, these factors should be considered for complete understanding of the fracture behaviors in the actual HAZ.

References

[1] J.-B. Lee, J.-K. Han, J. Korean Weld. Soc. 13 (1995) 34–41.
[2] J.I. Kim, C.K. Syn, J.W. Morris, Jr, Metall. Trans. A 7 (1983) 93–103.
[3] B.C. Kim, S. Lee, N.J. Kim, D.Y. Lee, Metall. Trans. A 22 (1991) 139–149.
[4] D.P. Fairchild, Fatigue and Fracture Testing of Weldments, ASTM STP 1058, American Society for Testing and Materials, Philadelphia, 1990, pp. 117–141.
[5] M. Toyoda, J. Jpn. Weld. Soc. 62 (1993) 603–616.
[6] C.L. Davis, J.E. King, Metall. Trans. A 25 (1994) 563–573.
[7] S. Lee, B.C. Kim, D. Kwon, Metall. Trans. A 23 (1992) 2803–2816.
[8] F. Minami, M. Toyoda, C. Thaulow, M. Hauge, Q. J. Jpn. Weld. Soc. 13 (1995) 508–517.
[9] K. Masubuchi, Analysis of Welded Structures (chapter 2), Pergamon Press, New York, NY, 1980.
[10] H. Ikawa, H. Oshige, T. Tanoue, J. Jpn. Weld. Soc. 49 (1980) 467–472.

[11] EEMUA Standard No. 147, Recommendation for the Design and Construction of Refrigerated Liquefied Gas Storage Tanks, The Engineering Equipment and Materials Users Association, 1986.
[12] British Standard 7777, Flat-bottomed, Vertical, Cylindrical Storage Tanks for Low Temperature Service, British Standards Institution, 1993.
[13] B. Fultz, J.I. Kim, Y.H. Kim, H.J. Kim, G.O. Fior, J.W. Morris, Jr, Metall. Trans. A 16 (1985) 2237–2249.
[14] E.F. Nippes, J.P. Balaguer, Weld. J. 65 (1986) 237s–243s.
[15] J.-i. Jang, Y.-C. Yang, W.-S. Kim, D. Kwon, Adv. Cryog. Eng. 44 (1998) 41–48.
[16] Y. Nakao, H. Oshige, S. Noi, Y. Nishi, Q. J. Jpn. Weld. Soc. 3 (1985) 773–781.
[17] B. Jofesson, H.O. Andren, Proceedings of the International Conference on Recent Trends in Welding Science and Technology, Gatlinburg, Tennessee, May 1989, pp. 243–250.
[18] H. Okada, K. Ikeuchi, F. Matsuda, I. Hrivnak, Z. Li, Q. J. Jpn. Weld. Soc. 12 (1994) 236–242.
[19] Y. Kozimo, Y. Fukada, Q. J. Jpn. Weld. Soc. 6 (1988) 41–46.
[20] I. Hrivnak, F. Matsuda, Z. Li, K. Ikeuchi, H. Okada, Trans. JWRI 21 (1992) 101–110.
[21] J.H. Chen, Y. Kikuta, T. Araki, M. Yoneda, Y. Matsuda, Acta Metall. 32 (1984) 1779–1788.
[22] S. Banerjee, Eng. Frac. Mech. 15 (1981) 343–390.
[23] B.-W. Lee, J.-i. Jang, D. Kwon, Mater. Sci. Eng. A, (in press).